Nanochem Res 7(2):107-121, Summer and Autumn 2022

RESEARCH PAPER

Adsorption of Cationic Dye from Aqueous Solutions by Green pH Responsive Hydrogels Based on Poly(2-acrylamido-2-methyl-1-propanesulfonic acid)

Hamidreaz Muhammadi [1], Massomeh Ghorbanloo [1,*], Masami Mori [2], Hidenori Yahiro [2]

[1] *Department of Chemistry, Faculty of Science, University of Zanjan, Zanjan, Iran.*

[2] *Department of Materials Science and Biotechnology, Graduate School of Science and Engineering, Ehime University, Matsuyama, Japan.*

ARTICLE INFO

Article History:
Received 16 March 2022
Accepted 18 March 2022
Published 1 May 2022

Keywords:
pH responsive
1-Vinylimidazole, 2-Acrylamido-2-methyl-1-propane sulfonic acid
Rhodamine B adsorption
Quaternization

ABSTRACT

Poly(2-acrylamido-2-methyl-1-propanesulfonic acid-*co*-1-vinylimidazole), hydrogels were synthesized via free radical polymerization reaction at different conditions and modified with di-alkyl halide. P(AMPS-Na^+-*co*-VIm)-Ag and p(AMPS-H^+-*co*-VIm)-Ag were prepared by reducing $Ag(CH_3COO)$ salts loaded into p(AMPS-Na^+-*co*-VIm) and p(AMPS-H^+-*co*-VIm) hydrogels and then reduced by $NaBH_4$. Metal nanoparticles embedded p(AMPS-Na^+-*co*-VIm)-Ag and p(AMPS-H^+-*co*-VIm)-Ag were visualized by high resolution X-ray photoelectron spectroscopy (HRXPS) and transmission electron microscopy (TEM). The prepared porous hydrogels and related composites were utilized in the adsorption of Rhodamine B from aqueous solutions. Among non-quaternized hydrogels, p(AMPS-Na^+-*co*-VIm) and its composite outperformed p(AMPS-H^+-*co*-VIm) and p(AMPS-H^+-*co*-VIm)-Ag. since high porosity increases absorption capacity, which depends on the size and shape of the pores. In addition, the effect of 1,4-dibromobutane quaternization on the catalytic performance of nano-composites was investigated. Finally, the catalyst was easily recovered from the reaction medium and re-used for a further four runs without significant loss of activity. The durability of the catalyst structure without leaching was confirmed by FT-IR spectra and atomic absorption spectroscopy, respectively.

How to cite this article
Muhammadi H., Ghorbanloo M., Mori M., Yahiro H. Adsorption of Cationic Dye from Aqueous Solutions by Green pH Responsive Hydrogels Based on Poly(2-acrylamido-2-methyl-1-propanesulfonic acid). Nanochem Res, 2022; 7(2):107-121. DOI: 10.22036/ncr.2022.02.006

INTRODUCTION

The growing concern for a sustainable chemical industry has led researchers to reevaluate the fundamental aspects of production processes based on the principles of green chemistry [1]. The treatment of wastewaters is a key aspect of industrial sustainability. Environmental priority pollutants that require immediate attention include organic pollutants, synthetic dyes, and wastewater with low C/N ratios [2]. They pose a persistent threat to the entire ecosystem due to the poor water quality resulting from increased metal load, resistance to degradation, and propensity for bio-magnification [3]. It is essential to address their containment below the permissible limit from major point sources, such as industries, sewage waste, *etc.*, which impact groundwater quality. In this regard, the design and development of new polymeric adsorption matrixes that can provide an economical and efficient treatment technology have recently become the focus of research [4].

Green nanomaterials have attracted significant attention and play a crucial role in water treatments due to their unique large surface-to-volume ratios, high porosity, and high removal

* Corresponding Author Email: *m_ghorbanloo@znu.ac.ir*

rates, which serve as environmentally friendly water-pollutant adsorbents [5]. In addition, there are various opportunities and challenges facing scientists for using nanomaterials in purification and desalination of water due to their toxicity and environmental regulations. Numerous types of green nanomaterials have been used to purify waste water from toxic organic and inorganic pollutants such as noble metal nanoparticles like silver and gold [5].

Another viable strategy to remove dyes from wastewaters is adsorption, by which dye-polluted waters are treated with porous materials called sorbents. This approach is convenient since it is less costly and allows for regenerating sorbents for multiple reuses. Ideal sorbents possess large surface area, high adsorption capacity, and a porous structure [1]. Consequently, interest in nanostructured sorbents, which meet the aforementioned criteria, has recently increased. Such materials include graphene oxide, carbon nanotubes, and chitosan. Supramolecular gels are another promising class of nanostructured materials for the purpose of dye removal from wastewaters. Nowadays polymers are employed in a multidisciplinary field of research. Hydrogels are being used in diverse sectors such as biomedical engineering, food technology, agricultural engineering, and water resource engineering [6-8]. Hydrogels offer a large-scale flexibility in terms of fast swelling kinetics, modifiable surface characteristics such as charge, functionality, fast diffusion process, large area, controllable pore structure, permeability catalysis, fast kinetics, thermo-stability, interesting acid/base properties, and hydrophilicity [6]. In water treatment applications, hydrogels are found to be very effective for the containment of a broad class of organic and inorganic aqueous pollutants including metal ions, noxious dyes, and pestilential pharmaceutical wastes [7].

Hydrogel systems with AMPS moiety are pH sensitive. Ajmal *et.al* investigated the effect of high pH on p(NIPAM-AMPS) and its catalytic activity [8]. According to their results, at low pH, the particle size was very small, in the range of 80 nm. With an increase in pH, the hydrodynamic diameter increased and particle size reached 190 nm. Such an increase in hydrodynamic diameter was observed due to the repulsion between negative charges on polymeric network which are produced due to the deprotonation of sulfonic groups at higher pHs. The negatively charged sulfonic groups act as repellents among the polymer chains in p(NIPAM-AMPS) network, resulting in swelling the network and increasing the particle size at higher pHs of the medium. This system respond by swelling and shrinking of its network, which can influence the diffusion speed of reactants towards the surface of nanocatalysts and, in turn, can affect the catalytic activity of the nanoparticle composites. It is obvious that both the pH and temperature do not affect the nanoparticles Ag or Pd embedded in p(NIPAM-AMPS) but influence the p(NIPAM-AMPS) network.

In this context, the current work was designed to explore the potential of p(AMPS-Na^+-*co*-VIm), p(AMPS-H^+-*co*-VIm) and 1,4-BB-p(AMPS-Na^+-*co*-VIm) bulk hydrogel in the fabrication of metal nanoparticles and subsequently as reactor media in the removal of Rh B from aqueous media. More interestingly, the p(AMPS-Na^+-*co*-VIm) catalyst can be easily separated after catalytic reaction and readily recycled over four successive reaction cycles. This eco-friendly and inexpensive catalyst is catalytically effective with superior recyclability.

EXPERIMENTAL SECTION

Materials and Equipment

The monomers, 2-acrylamido-2-methyl-1-propanesulfonicacid(AMPS-H^+)and2-acrylamido-2-methylpropane sulfonic acid sodium salt (AMPS-Na^+) solution 50%, as ionic monomer (98%, Sigma Aldrich), 1-Vinylimidazole (1-VIm) (99%, Sigma Aldrich) as monomers, the crosslinker, N, N′-methylenebisacrylamide (MBA) (99%, Across), the initiators, 2,2′-azobis(isobutyronitrile) (AIBN) (99%, Sigma Aldrich) and the accelerator N,N,N′,N′-tetramethylmethylenediamine (TEMED) (98% Across) were used in hydrogel preparation. $Ag(CH_3COO)$ (Merck) was employed as a metal ion source. Sodium borohydride ($NaBH_4$, 98%, Merck) was used in the reduction of metal ions for preparing metal nanoparticles. All the chemicals were utilized as received without further purification. FT-IR spectra were recorded in KBr disks with a Bruker FT–IR spectrophotometer. The exact amount of the silver in the composites was determined by Varian Spectra 220 AA spectroscopy. The morphology of swollen p(AMPS-*co*-VIm) and p(NaAMPS-*co*-VIm) hydrogels was investigated with Scanning Electron Microscopy (SEM) via MIRA3 TESCAN FE SEM and an accelerating voltage of 10 keV. The sample was swollen and quickly frozen in liquid nitrogen. The hydrogel

was freeze-dried at -50 °C for 3 days to preserve its porous structure without any collapse. After that, the dried samples were deposited onto an aluminum stub and sputter-coated with gold for 60 s for enhancing conductivity. Transmission electron microcopy (TEM, PHILIPS CM-30) was applied for determining the size of metal nanoparticles inside the hydrogel nanocomposites. Particles in ethanol was sonicated and 5 µL suspension was immediately transferred to Cu grids completely covered with carbon, and dried under room conditions. They were analyzed in a Jeol 200 KeV field emission transmission electron microscopy and electron diffraction data were supported by EDS obtained on single nanoparticles. High resolution X-ray photoelectron spectrum (HRXPS) was performed by a 1600E Perkin Elmer applying Mg-Kα excitation source. The reaction products of oxidation were determined and analyzed using an HP Agilent 6890 gas chromatograph equipped with a HP-5 capillary column (phenyl methyl siloxane 30 m × 320 µm × 0.25 µm).

Preparation of hydrogels

Neutral reaction solution

Synthesis of p(AMPS-Na$^+$-*co*-VIm) hydrogels was carried out via free radical polymerization reaction techniques at 65 °C, with different mole ratios of NIPAm and AMPS-Na$^+$ monomers, as shown in Scheme 1a. In the synthesis of p(AMPS-Na$^+$-*co*-VIm) hydrogel, 0.16 mL (0.85 mmol) AMPS-Na$^+$, 0.03 mL (0.36 mmol) 1-VIm were mixed, 0.015 g (5% monomer, 0.1 mmol) MBA, and 50 µL TEMED were added as crosslinking agent and accelerator, respectively. The polymerization reaction was initiated by adding the prepared AIBN solution of 0.0075 g (10% monomer, 0.045 mmol) in 0.75 mL ethanol. The mixture was transferred to

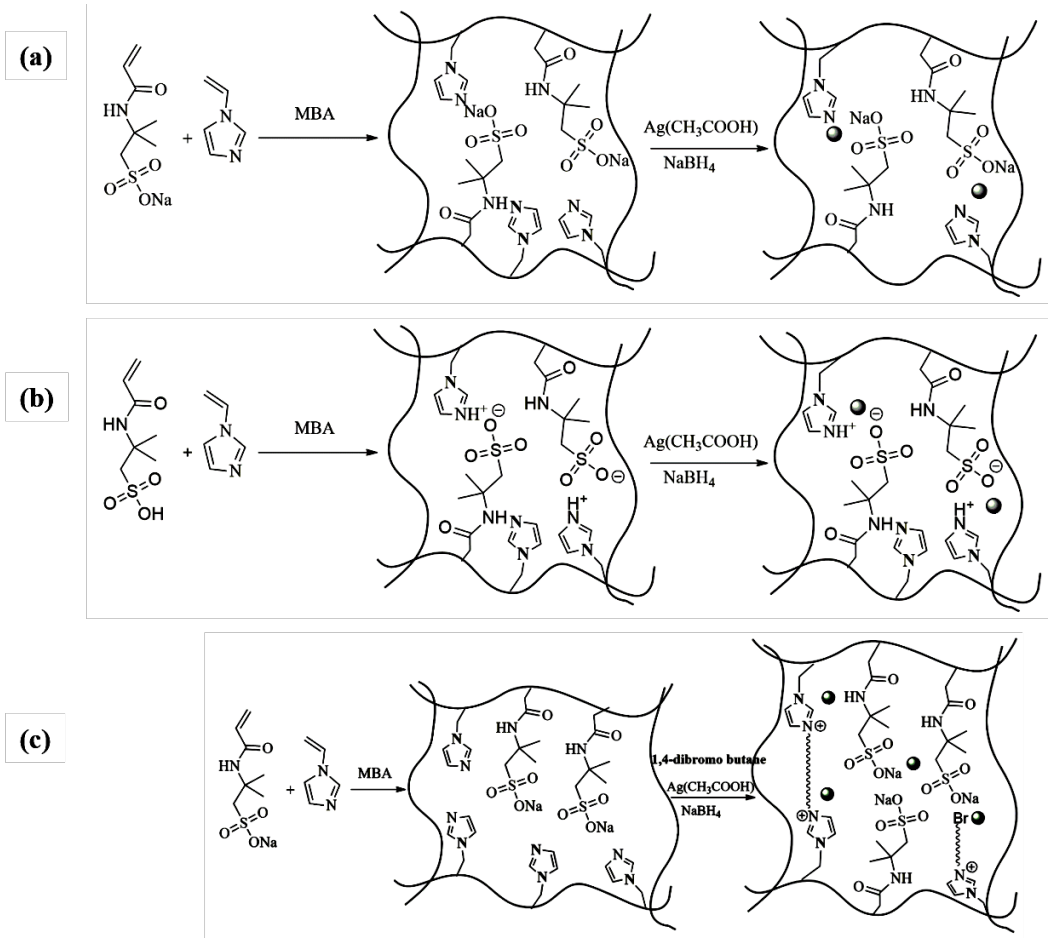

Scheme 1. Schematic representation of a) p(AMPS-Na$^+$-*co*-VIm)-Ag nano-composites, b) p(AMPS-H$^+$-*co*-VIm)-Ag nano-composites preparation and c) modification of p(AMPS-Na$^+$-*co*-VIm) hydrogel with 1,4-dibromo butane.

plastic straws (~ 4 mm in diameter), and kept as such for 4 h at 65 °C to complete polymerization and crosslinking. Finally, the obtained 3-D hydrogels were kept submersed in water for 24 h. After the cleaning procedure, hydrogels were dried in an oven at 40 °C till constant weight.

Selected FT-IR (KBr, cm^{-1}): (p(AMPS-Na^+-*co*-VIm)): 3450 (br, s), 3107 (shoulder), 2989 (w), 2933 (w), 1662 (vs), 1547 (s), 1393 (m), 1372 (w), 1302 (w), 1225 (m), 1193 (w), 1161 (w), 1119 (m), 1087 (w), 1051 (s), 915 (w), 862 (w), 819 (w), 766 (w), 670 (w), 627 (m), 531 (w).

Acidic reaction solution

In the synthesis of p(AMPS-H^+-*co*-VIm) hydrogels, 0.124 g (0.6 mmol) AMPS, 0.054 mL (0.6 mmol) 1-VIm, 0.015 g (5% monomer, 0.1 mmol) MBA, and 50 µL TEMED were mixed with 0.5 mL ethanol and to this solution a separately prepared AIBN solution of 0.005 g (5.5% monomer, 0.033 mmol) AIBN in 0.25 mL ethanol was added and vortexed homogeneously, as shown in Scheme 1b. The mixture was placed into plastic straws (~ 4 mm in diameter) which were immersed in a 65 °C water bath for 4 h to complete polymerization and crosslinking. The mixture was transferred to plastic straws (~ 4 mm in diameter), and kept as such for 4 h at 65 °C to complete polymerization and crosslinking. Finally, the obtained 3-D hydrogels were kept submersed in water for 24 h. After the cleaning procedure, hydrogels were dried in an oven at 40 °C till constant weight.

Selected FT-IR (KBr, cm^{-1}): (p(AMPS-H^+-*co*-VIm)): 3529 (br, s), 3129 (w), 3065 (w), 2979 (w), 2937 (w), 2862 (w), 1662 (s), 1544 (s), 1463 (m), 1393 (w), 1369 (w), 1305 (m), 1230 (w), 1187 (w), 1155 (w), 1113 (w), 1091 (m), 1037 (vs), 908 (w), 854 (w), 822 (w), 769 (m), 664 (w), 625 (s), 523 (w), 459 (w).

In situ synthesis of metal nanoparticles within p(AMPS-H^+-co-VIm) and p(AMPS-Na^+-co-VIm) hydrogels

A series of Ag loaded on p(AMPS-H^+/AMPS-Na^+-*co*-VIm)–Ag were prepared via the impregnation-reduction method in aqueous medium using $NaBH_4$ as a reducing agent. Specifically, p(AMPS-H^+/AMPS-Na^+-*co*-VIm) (0.25 g) was immersed in an aqueous solution of 500 ppm $Ag(CH_3COO)$ and stirred continuously at 25 °C for 24 h. The metal ions loaded hydrogel was then filtered and washed with deionized water to remove loosely-bound silver ions. Silver ions loaded in hydrogels were reduced by using 0.1 M aqueous solution of $NaBH_4$ for 3 h. The resultant Ag catalyst was filtered and washed with deionized water for three times. The catalyst was finally obtained after drying under vacuum at 40 °C overnight (Scheme 1). The amounts of metal nanoparticles entrapped in hydrogels were calculated by AAS measurements after the dissolution of metal nanoparticles embedded within hydrogel by treating with HNO_3 aqueous solution.

Quaternization of hydrogel

To create a positive charge on p(AMPS-Na^+-*co*-VIm) hydrogels, the modification agent 1,4-BB reacted with p(AMPS-Na^+-*co*-VIm) hydrogels, as shown in Scheme 1c. In the quaternization reaction, about 0.1 g dried hydrogels were treated with 1,4-BB (0.56 mL) in 20 mL ethanol mixtures at 50 °C at 200 rpm mixing rate for 24 h. Then the quaternized hydrogels were washed with plenty of acetone for removing the unreacted reactants from the hydrogel matrices, and, finally, quaternized p(AMPS-Na^+-*co*-VIm) hydrogels, (Q- p(AMPS-Na^+-*co*-VIm)), were dried in an oven at 40 °C.

Selected FT-IR (KBr, cm^{-1}): (p(AMPS-Na^+-*co*-VIm)-BB): 3442 (br, s), 3246 (shoulder), 3136 (w), 3082 (w), 2916 (m), 2851 (w), 1657 (s), 1565 (m), 1555 (m), 1500 (w), 1449 (m), 1365 (w), 1226 (w), 1164 (s), 1107 (w), 1086 (m), 1029 (w), 951 (w), 910 (w), 835 (m), 754 (m), 655 (m), 618 (w), 529 (w).

Determination of the amount of silver within hydrogel matrix

The amount of metal ion within the hydrogel matrix was determined by using Atomic Absorption Spectroscopy using metal ion solution obtained by treating 25 mg p(AMPS-H^+-*co*-VIm)-Ag and p(AMPS-Na^+-*co*-VIm)-Ag with 4 mL HNO_3 three times for 18 h to dissolve Ag ions.

Adsorption study

The potential of prepared bare and composite hydrogels for using as adsorbent was investigated by conducting the adsorption studies of Rhodamine B from water. The effect of various factors on the adsorption of Rh B, such as different doses of hydrogel, and the effect of solution pH on the adsorption of dye were explored systematically to obtain optimized adsorption circumstances. The effect of pH on dye adsorption was examined over the pH range of 2–11 and the pH was changed by

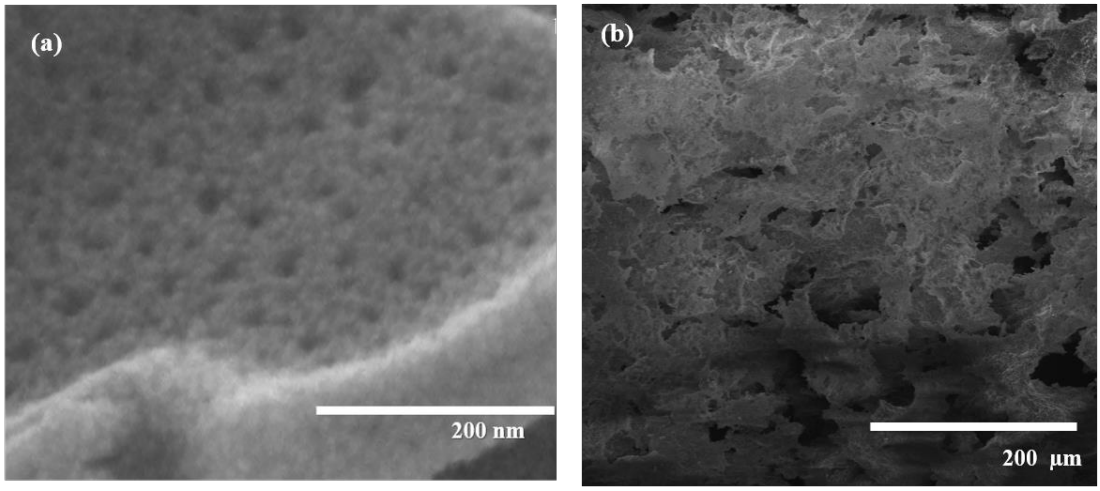

Fig. 1. SEM image of a) p(AMPS-H^+-*co*-VIm) hydrogels, b) p(AMPS-Na^+-*co*-VIm) hydrogels.

using 0.1 M NaOH and 0.1 M HCl solutions. In the common adsorption research, 0.1 g of hydrogel was added in 40 mL dye solutions (40 mg/L) for 24 h. The adsorption process was performed at room temperature with constant magnetic stirring. 1 ml sample was removed from the reaction mixture at different times. Then, these samples were diluted with distilled water about 3 times. This dilution was related to the initial concentration of each sample. After 24 h, the hydrogel was removed and filtered. The concentration of the Rh B remained in the dye solutions was determined by using UV/Vis spectrophotometer at 554 nm as λ_{max} of Rh B. The adsorption efficiency or percentage removal was calculated by applying the following equation [9, 10]:

$$\text{Removal\%} = (C_0 - C_e)/C_0 \times 100 \qquad (1)$$

where C_o and C_e are the initial and equilibrium concentration of dye solutions (mg/L), respectively [11]. After achieving the proper pH, the effect of adsorbent dose on the adsorption capacity was examined by different amounts of hydrogel from 0.05 to 0.2 g at pH 2 under equal experimental circumstances; the percentage removal was explored by applying Eq. (1).

Selected FT-IR (KBr, cm^{-1}): (p(AMPS-Na^+-*co*-VIm)): 3450 (br, s), 3107 (shoulder), 2989 (w), 2933 (w), 1662 (vs), 1547 (s), 1393 (m), 1372 (w), 1302 (w), 1225 (m), 1193 (w), 1161 (w), 1119 (m), 1087 (w), 1051 (s), 915 (w), 862 (w), 819 (w), 766 (w), 670 (w), 627 (m), 531 (w).

Selected FT-IR (KBr, cm^{-1}): (p(AMPS-Na^+-*co*-VIm)/Rh b): 3479 (br), 3133 (w), 2986 (w), 2934 (w), 2861 (w), 2735 (w), 2620 (w), 1671 (vs), 1545 (s), 1456 (m), 1393 (m), 1376 (w), 1302 (w), 1185 (m), 1103 (w), 1038 (vs), 901 (w), 857 (w), 812 (w), 770 (w), 665 (shoulder), 627 (m), 518 (w).

RESULTS AND DISCUSSION

Synthesis and Characterization

The characterization of porous p(AMPS-H^+-*co*-VIm) and p(AMPS-Na^+-*co*-VIm) hydrogels and their metal composites were carried out with various characterization techniques including SEM images, FT-IR spectroscopy, HRXPS, TEM images, EDX and AA spectroscopy.

The structure of p(AMPS-H^+-*co*-VIm) and p(AMPS-Na^+-*co*-VIm) hydrogels were determined using a Scanning Electron Microscope (SEM, JEOL 2010) on thin sections of freeze dried p(AMPS-H^+-*co*-VIm) and p(AMPS-Na^+-*co*-VIm) hydrogels, as shown in Fig. 1-a, b, respectively. The SEM image of p(AMPS-Na^+-*co*-VIm) indicates the formation of homogeneous (Fig. 1-c, d) and highly porous material in comparison with p(AMPS-H^+-*co*-VIm) hydrogel (Fig. 1-a, b).

The representative FT-IR spectra of p(AMPS-Na^+-*co*-VIm) and p(AMPS-H^+-*co*-VIm) are shown in Fig. 2 and Table 1. Both spectra showed absorption peaks at around 3000-3500 cm^{-1} stretching frequency of the O-H and N-H groups [12], and the bands at 2989 and 2933 cm^{-1} correspond to aliphatic -CH stretching. A sharp peak of C=O stretching of the amide I at around 1664 cm^{-1} (Fig. 2-a) and 1663 cm^{-1} (Fig. 2-c) and a strong peak of the N-H bending of amide II at 1547

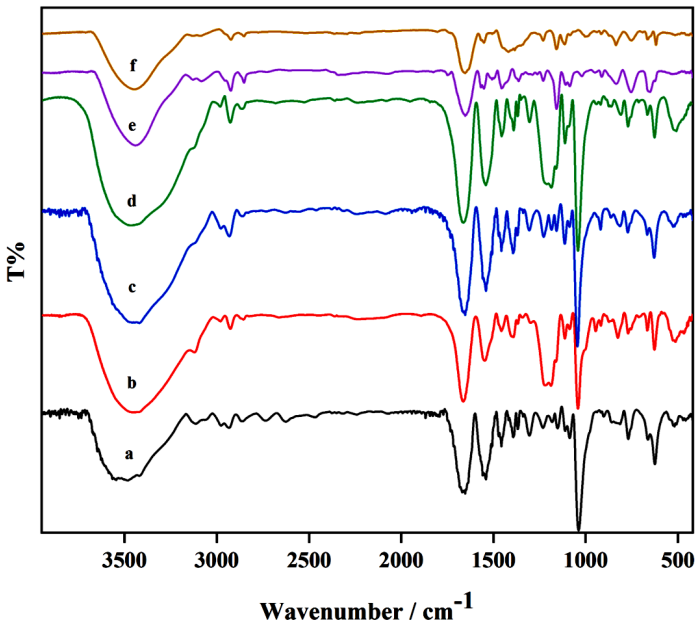

Fig. 2. FT-IR spectra of a) p(AMPS-Na$^+$-*co*-VIm), b) p(AMPS-Na$^+$-*co*-VIm)-Ag, c) p(AMPS-H$^+$-*co*-VIm), d) p(AMPS-H$^+$-*co*-VIm)-Ag, e) p(AMPS-Na$^+$-*co*-VIm)-BB, f) p(AMPS-Na$^+$-*co*-VIm)-BB-Ag.

cm^{-1} (Fig. 2-a) and 1542 cm^{-1} (Fig. 2-c). The relative weak peaks at 1460 cm^{-1} (Fig. 2-a) and 1453 cm^{-1} (Fig. 2-c) along with those at 1664 cm^{-1} and 1663 cm^{-1} are the symmetrical and asymmetrical $C(=O)_2$ stretching. Importantly, the sharp and strong peaks of the S=O stretching of AMPS-Na$^+$ and AMPS-H$^+$ at 1051 cm^{-1} (Fig. 2-a) [13] and 1037 cm^{-1} (Fig. 2-c) [14] were observed, respectively. Another two strong and sharp peaks at 1182 cm^{-1} (Fig. 2-a) and 1186 cm^{-1} (Fig. 2-c) resulted from the C-C(=O)-O stretching. A relatively broad and strong peak at 3456 cm^{-1} (Fig. 2-a) is attributed to the NH or OH stretching of p(AMPS-Na$^+$-*co*-VIm) where that for p(AMPS-H$^+$-*co*-VIm) (Fig. 2-c) becomes very broad at 3415 cm^{-1} since the OH group in the free acid superimposed the NH stretching of acrylamide moiety. Finally, the chemical changes in the structure of p(AMPS-Na$^+$-*co*-VIm)-Ag and p(AMPS-H$^+$-*co*-VIm)-Ag composites were confirmed via FT-IR spectroscopy. After loading Ag ions and reducing to Ag nano-particles, the small shifts in FT-IR spectra of compounds are related to the interactions between Ag and hydrogel matrix, as shown in Fig. 2 and b-d.

A schematic representation of metal loading and in situ reduction process for the formation of metal nanoparticles inside hydrogel networks are demonstrated in Schemes 1 and 2. TEM measurement was carried out for investigating the nanostructure of the sample. The TEM images of metal nanoparticles-containing p(AMPS-Na$^+$-*co*-VIm) and p(AMPS-H$^+$-*co*-VIm) hydrogels are given in Fig. 3 a-b. As can be seen, metal nanoparticles with a uniform spherical shape (about <20 nm)

Table 1. Specific bands in FT-IR spectra of hydrogels.

Compound	p(AMPS-Na$^+$-*co*-VIm)	p(AMPS-H$^+$-*co*-VIm)	p(AMPS-Na$^+$-*co*-VIm)-BB
O-H	3450	3529	3442
N-H	3107	3129	3136
C=O	1664	1663	1657
N-H bending of amide II	1547	1542	1555
S=O	1051	1037	1029
-N-C	------	----------	1560
–C-H	-------	----------	1360
C–N stretching	----------	----------	1160
–C=O	1662	1662	1657

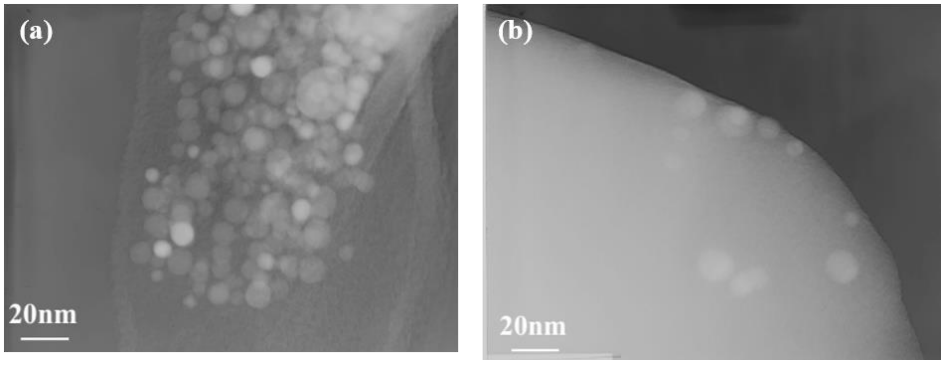

Fig. 3. TEM images of metal nanoparticles from a) p(AMPS-Na^+-*co*-VIm)-Ag and b) p(AMPS-H^+-*co*-VIm)-Ag.

are distributed within p(AMPS-Na^+-*co*-VIm) and p(AMPS-H^+-*co*-VIm)-Ag hydrogel matrices.

HRXPS analysis was applied to further investigate the interactions of metal nanoparticles with hydrogel functional groups. The exact binding energy of an electron is determined by three factors: the level of photoemission, the formal oxidation state of the atom, and the characteristics of the environment. To analyze these factors, the HRXPS spectra would be of great help since this technique can differentiate various oxidation states and chemical environments. In elevated positive oxidation states, an additional columbic interaction takes place between the photoemitted electron and the ion core, which generates a greater amount of binding energy.

The Ag 3d spectrum of the p(AMPS-Na^+-Ag) nanocomposite (Fig. 4) confirmed the presence of Ag with zero oxidation state in the hydrogel matrix. This result revealed that the organic moieties and Ag-NPs were incorporated into the structure of the hydrogel. The wide scan spectrum indicates that the Ag 3d doublet peaks were formed, which confirms the generation of Ag nanoparticles in the p(AMPS-Na^+-*co*-VIm)-Ag nanocomposite. Two peaks appeared: a peak pertaining to the Ag $3d_{3/2}$ transition at 374.87 eV and a peak corresponding to the Ag $3d_{5/2}$ transition at 368.86 eV. The development of these peaks can be ascribed to either the formation of Ag-N bonds or the interaction of the metal atoms and the functional groups in the *co*-polymer. The calculated spin energy between the two peaks was 6.01 eV. It can be stated that metallic Ag nanoparticles are formed and the Ag nanoparticles have a zero oxidation state [15,16]. In comparison with the standard binding energies of pure Ag (368.0 and 374.0 eV), the obtained binding energies of the Ag 3d peaks (Ag $3d_{3/2}$ and Ag $3d_{5/2}$) were higher because electrons in metallic silver were transferred to the functional groups of the hydrogel. Hence, it can be declared that there was an interaction between the Ag nanoparticles and the functional groups of the hydrogel, and the Ag nanoparticles were successfully generated in the hydrogel network.

The representation of the modification mechanism of porous p(AMPS-Na^+-*co*-VIm) hydrogels is given in Scheme 1c. After quaternization, the chemical changes in the structure of p(AMPS-Na^+-*co*-VIm) hydrogels were confirmed via FT-IR spectroscopy by recording the FT-IR spectra Q-p(AMPS-Na^+-*co*-VIm) as seen in Fig. 2-e. After quaternization, -N-C and –C-H bending coming from newly quaternized ^+NR (R: C_2H_4) groups were observed at 1560 cm^{-1} and 1360 cm^{-1}. The intensities of these peaks increased according to the length of alkyl chain, respectively. Furthermore, the new absorption band that occurred at 1160 cm^{-1} upon quaternization corresponded to C–N stretching. This new peak confirmed the interaction between the methyl group and the N atom in the ring [17]. The intensity of this stretching increased with quaternization. The –C=N and –C=C bands in aromatic rings were observed for each modified polymer.

The amount of metal ion within the hydrogel matrix was determined by using Atomic Absorption Spectroscopy after HNO_3 treatment; the amounts of silver were 0.198 mmol/g hydrogel for p(AMPS-Na^+-*co*-VIm)-Ag/H_2O, 0.042 mmol/g hydrogel for p(AMPS-H^+-*co*-VIm)-Ag/H_2O, and 0.283 mmol/g hydrogel for p(AMPS-Na^+-*co*-VIm)-BB-Ag composites, respectively.

Adsorption Studies

The prepared p(AMPS-Na^+-*co*-VIm) hydrogel

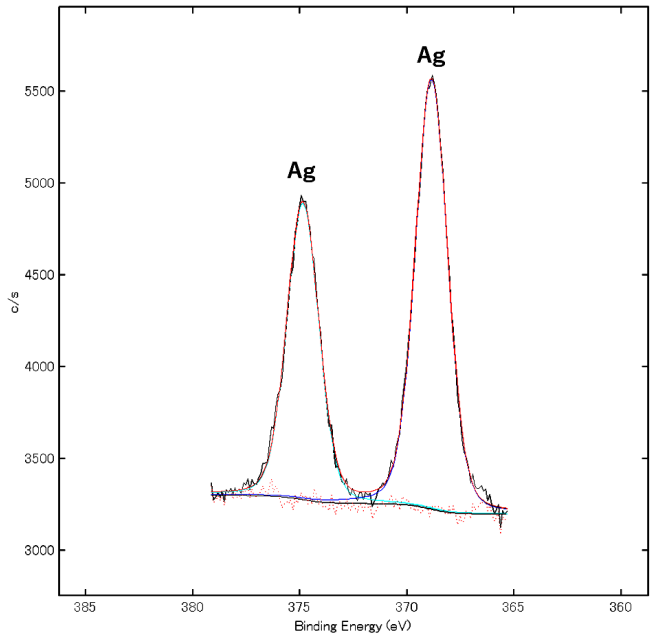

Fig. 4. HRXPS spectra of Ag 3d of p(AMPS-Na^+-*co*-VIm)-Ag.

was employed as adsorbent for the adsorptive removal of Rh B from aqueous medium. Fig. 5 illustrates variations in the adsorption capacity of Rh B at 25 °C. As depicted in Fig. 5, the adsorption efficiency of the Rh B molecules on the hydrogel enhanced with time. After 4 hours, this capacity achieved equilibrium, and beyond this point, no considerable change in the adsorption capacity of the Rh B molecules was observed.

At first, the effect of pH was investigated since variations in the pH value of dye solutions play a critical role in the adsorption process, which can change the surface charge of the poly(AMPS-Na^+-*co*-VIm) and the degree of ionization of dye molecule [18].

Various types of dyes can generate different pH values based on the characteristics of the utilized adsorbent [19]. In this study, the pH level ranging from 2.0 to 11.0 was considered to examine the role of pH in the adsorption efficiency of Rh B on the poly(AMPS-Na^+-*co*-VIm) hydrogel (Fig. 6-a). As mentioned above, the initial pH of the solution determines the adsorption level of poly(AMPS-Na^+-*co*-VIm). The results demonstrate that a boost in the pH level from 2.0 to 11.0 led to a gradual reduction in the adsorption capacity of poly(AMPS-Na^+-*co*-VIm) from 68% to 25%. The absorption capacity of Rh B on poly(AMPS-Na^+-*co*-VIm) differed from that of other adsorbents in previous studies [20,21].

This discrepancy can be ascribed to the surface charge of this adsorbent and structure of the Rh B molecule at different pHs (Scheme 2). To be more precise, the molecules had a monomeric structure at pH=2, which facilitated the penetration of these molecules into the cross-linked structure of poly(AMPS-Na^+-*co*-VIm) [22]. Moreover, the Rh B molecules is electropositive and the adsorbent possessed high-surface negative-charge density. Therefore, the electrostatic interaction between the Rh B molecules and -SO_3^- groups of the adsorbent was enhanced. When pH was greater than 2, Rh B had a zwitterionic structure. Under such conditions, the Rh B and larger molecules were aggregated, which decreased the density of Rh B's positive charge. Consequently, the Rh B molecules had trouble penetrating into the cross-linked structure, and the electrostatic interaction between these molecules and -SO_3^- groups of the adsorbent slowly dissipated. One possible explanation is that H^+ is released from the carboxylic groups of Rh B, which augments the repulsive force of the adsorbate and the sorbent. Therefore, a boost in the pH level from 2.0 to 11.0 reduces the adsorption efficiency of Rh B. To put another way, since -COOH groups on Rh B are ionized, due to an increase in pH levels, the electrostatic repulsion between the generated -COO^- groups on Rh B and the -SO_3^- groups on the hydrogel is raised. Thus, the Rh B molecules have difficulty permeating the hydrogel.

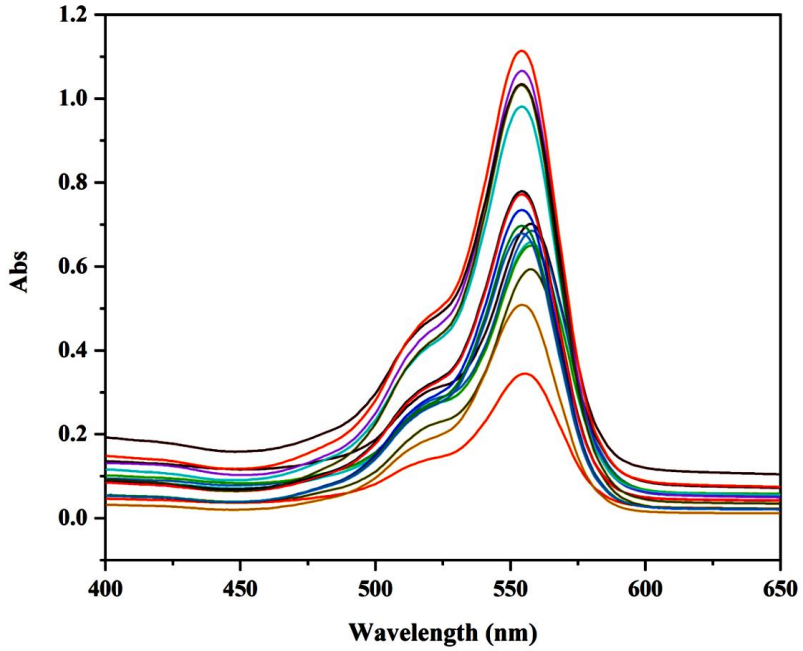

Fig. 5. UV-Vis spectra of Rh B adsorption by p(AMPS-Na$^+$-*co*-VIm)-Ag (0.1 g hydrogel, pH = 2, 40 ppm, Rh B, 4 h, R. T).

Fig. 6-b illustrates variations in the adsorption capacity of Rh B with respect to contact time. As depicted in Fig. 6, the adsorption efficiency of the Rh B molecules on the hydrogel was enhanced with time, and it reached equilibrium after 4 h. However, after this point, no considerable change in the adsorption efficiency of the Rh B molecules was observed. Initially, both -SO_3^- and the imidazole functional groups in the hydrogel were ready to interact with the cationic dye (Rh B) via electrostatic interactions, hydrogen bonding, and van der Waals forces [23,24]. During this process, the Rh B molecules diffused on the hydrogel surface and saturated all the functional groups. Hence, the adsorption efficiency gradually decreased and approached equilibrium.

By increasing the amount of p(AMPS-Na$^+$-*co*-VIm) hydrogel from 100 mg to 400 mg, the adsorption level of Rh B quickly declined. As more hydrogel (above 400 mg) was added, the

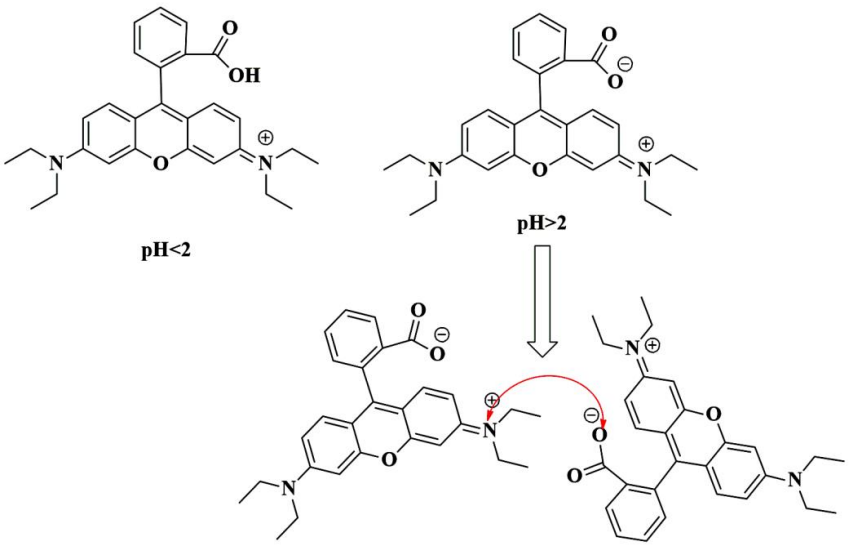

Scheme 2. Rh B molecule in different pH.

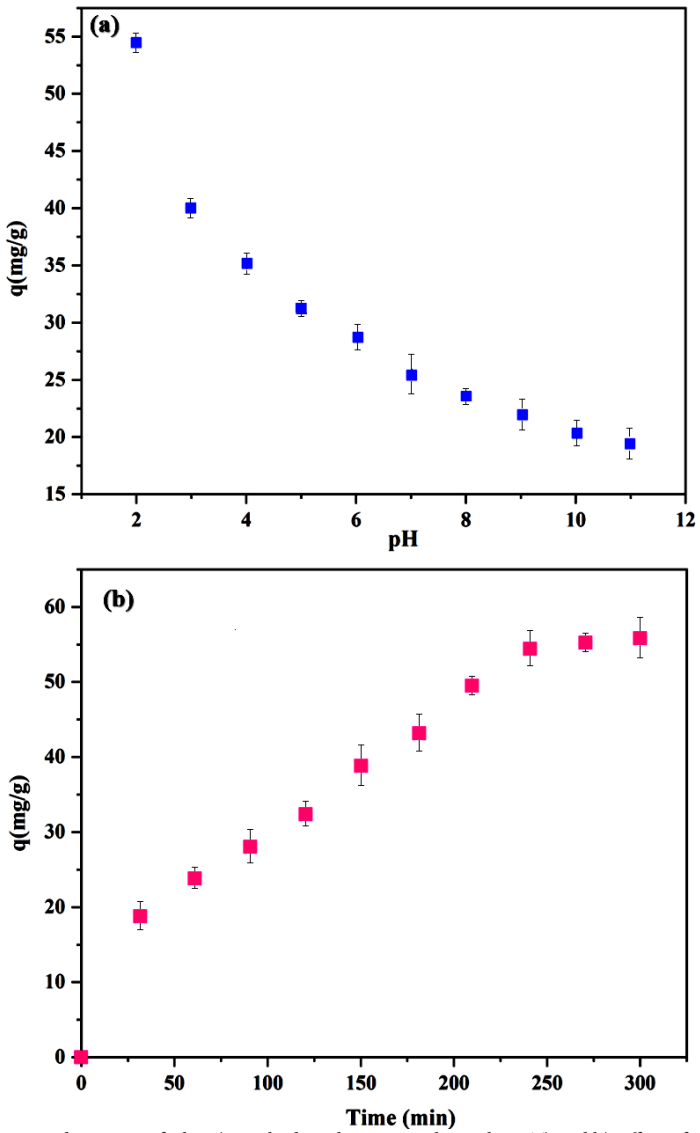

Fig. 6. a) Effect of pH value on adsorption of Rh B (0.1 g hydrogel, 40 ppm Rh B, 4 h, R. T) and b) Effect of contact time on adsorption of Rh B (0.1 g hydrogel, pH = 2, 40 ppm Rh B, R. T).

adsorption capacity gradually decreased till the equilibrium was reached. Although the surface area and accessible adsorption sites on the hydrogel rose with an increase in adsorbent dosage, so did the overlap between the active sites. Therefore, the number of accessible sites per unit mass diminished [25]. Furthermore, the Rh B molecules had a longer path to reach the active sites, which reduced the adsorption capacity. Thus, it can be declared that one of the most promising approaches for industrial wastewater treatment is batch charging. In addition, when an excessive amount of adsorbent (more than 4 mg) is used, the adsorption sites overlap.

The concentration of adsorbate solutions is another factor that affects adsorption capacity. Considering this issue, this study also examined variations in the initial concentration of adsorbate solutions. As for Rh B, three initial concentrations (10, 20, 40, and 80 ppm) were considered for the solution, and four mixtures were prepared. The adsorbent was 0.1 g of dried p(AMPS-Ag^{+}-*co*-VIm) hydrogel added to 40 mL of each solution. Fig. 7 shows the volumes of Rh B adsorbed per gram of dried p(AMPS-Ag^{+}-*co*-VIm) hydrogel with respect to time intervals. With a boost in the concentration of the adsorbate mixture from 10 to 80 ppm, the amount of adsorbed Rh B was raised from 36.2 to 55.1 mg/g, which indicates that the

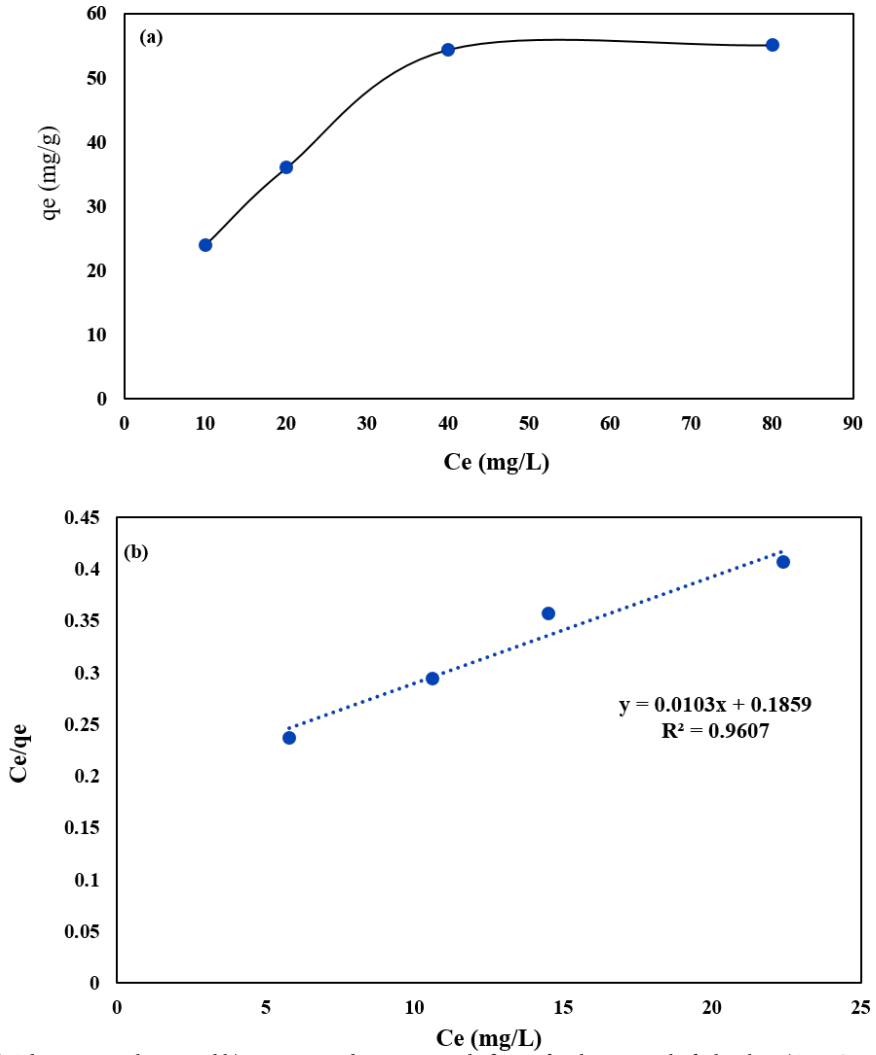

Fig. 7. a) Adsoption isotherm and b) Langmuir adsorption mode fitting for the removal of Rh B by p(AMPSNa-co-VIm) hydrogel.

solution with a low concentration cannot saturate the active adsorption sites of the adsorbent. On the other hand, as the concentration of the adsorbate solution rose, the active adsorption sites were slowly filled with Rh B which confirms the increment of adsorption efficiency.

Rh B has a molecular weight of 479.02 g/mol and a solubility of 20 g/L in water at room temperature. It has a higher tendency to separate from water and attach to the active adsorption sites due to its lower solubility. Another driving force behind adsorption is the surface charge of adsorbate and adsorbent, and Rh B possesses unit positive charges. Generally, dye molecules in the mixture are dispersed quickly on the surface of the adsorbent when the concentration of the dye is augmented [26]. Therefore, adsorption efficiency benefits from the increment of dye concentration. Concerning cationic dyes such as Rh B, strong electrostatic interactions are formed between negatively charged groups (like $-SO_3^-$) on composites and positively charged groups on dye molecules. Hence, with a boost in dye concentration, adsorption capacity is raised.

Furthermore, the effect of Ag nanoparticles in the adsorption capacity of the prepared hydrogel was investigated. Equivalent amounts of the bare hydrogel and silver nanocomposite were added in aqueous solutions of Rh B. The adsorption capacity obtained are 54.4 mg/g and 66.8 mg/g for p(AMPS-Na^+-*co*-VIm) hydrogel and p(AMPS-Na^+-*co*-VIm)-Ag composite, respectively. The results indicates that a greater amount of Rh B was adsorbed on the p(AMPS-Na^+-*co*-VIm)-Ag

composite. Additionally, the Ag nanoparticles on the hydrogel had great surface energy; therefore, the Rh B molecules were easily adsorbed by them. This phenomenon can be attributed to the greater binding affinity between the Ag nanoparticles and the Rh B molecules. Thus, the fabrication of Ag nanoparticles in p(AMPS-Na^+-*co*-VIm) hydrogel increases its adsorption capacity [27]. Decorating Ag-NPs onto the Rh B has shown to improve the adsorption capacity which can be attributed to the increase in its specific surface area. The augmentation of Ag nanoparticles increased the number of active adsorption sites on the surface of the hydrogel and elevated the adsorption capacity of Rh B [28].

There are three possible explanations for an increase in Rh B uptake. The first one has to do with the silver nanoparticles that are present on the backbone of the nanocomposite. They have a great tendency to interact with the Rh B molecules. The second explanation is that adding more Ag nanoparticles to the nanocomposite increases its thermal stability. The last one pertains to the formation of a highly crystalline nanocomposite owing to an increase in the number of Ag nanoparticles, which, in turn, promotes adsorption capacity [29].

The differences in the adsorption capacity can be attributed to the experimental condition, synthesized end-product such as functional groups present, and textural properties (pore size and volume) of the matrix system. The same results have been reported in some literatures. The recorded adsorption capacity were 47 and 55 mg/g for DAA/Ge hydrogel and DAA/Ge/Ag nanocomposite, respectively. It is evident that DAA/Ge/Ag nanocomposite exhibited greater adsorption capacity comparing with DAA/Ge hydrogel. This result demonstrates how silver nanoparticles can improve the adsorption performance of the hydrogel which represents an additional site for electrostatic interaction with cationic methylene blue (MB) molecules [30].

Scheme 3 illustrates the adsorption mechanism of cationic dyes on p(AMPS-Na^+-*co*-VIm) hydrogel. There is a strong interaction between negatively charged (SO_3^-) groups on the hydrogel with = N^+– moieties in cationic dyes. There are also other factors contributing to the improvement of the adsorption property of hydrogels such as van der Waals forces, hydrogen bonds, π-π stacking interactions, and hydrophobic interactions [31].

As shown in Fig. 8, the existence of these interactions is further confirmed by FTIR spectra of p(AMPS-Na^+-co-VIm) after adsorption. Compared to that of p(AMPS-Na^+-*co*-VIm) before adsorption, the peak of SO_3 groups of the hydrogel is shifted from 1051 to 1038 cm^{-1} after adsorption toward cationic dyes, which is due to the electrostatic interaction and hydrogen bonding between the SO_3 groups in AMPS-Na^+ and cationic dyes. Additionally, it is observed that the band of amide –C=O groups of the hydrogel is shifted from 1662 to 1671 cm^{-1} after adsorption toward cationic dyes. This is also because there are hydrogen bonds between MBA segment and COOH group of Rh B dye [32].

To compare the adsorption capacity of p(AMPS-

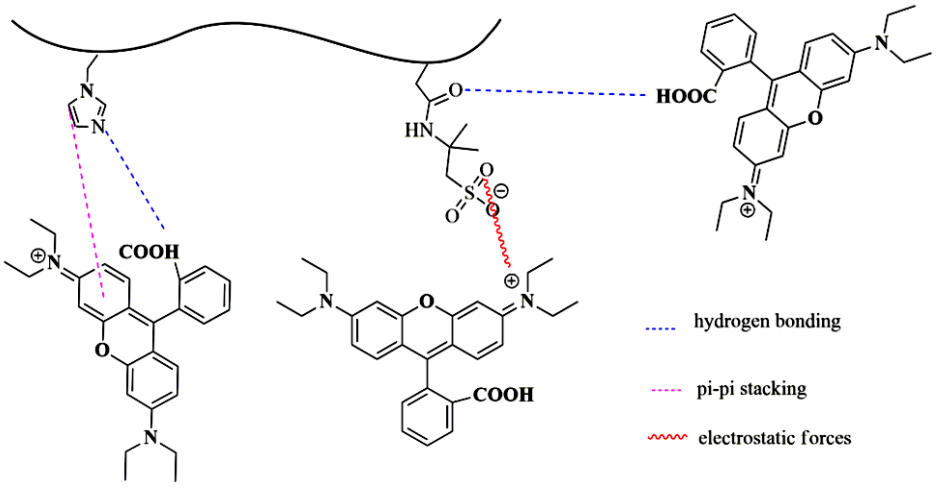

Scheme 3. Schematic interactions of Rh B onto the p(AMPS-Na^+-*co*-VIm) hydrogel.

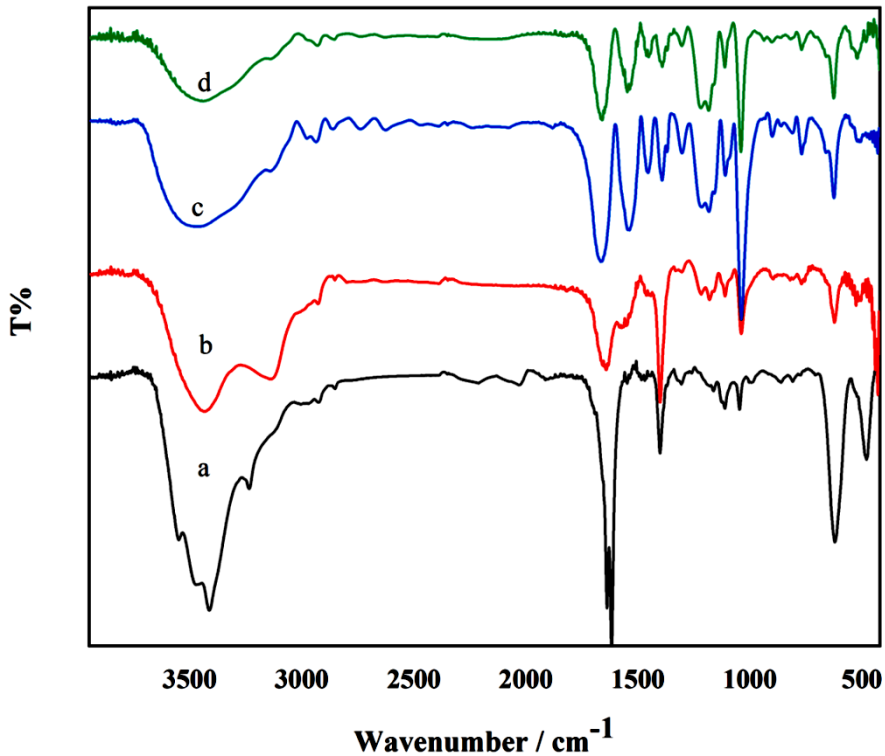

Fig. 8. FT-IR spectra of a) p(AMPS-Na$^+$-VIm) hydrogel, b) p(AMPS-Na$^+$-VIm)/Rh B (pH=2, 0.2 g), c) p(AMPS-Na$^+$-VIm)/Rh B (pH=3, 0.2 g), d) p(AMPS-Na$^+$-VIm)/Rh B (pH=3, 0.1 g).

Na$^+$-*co*-VIm) hydrogels with p(AMPS-H$^+$-*co*-VIm), we used the same amount of p(AMPS-H$^+$-*co*-VIm) hydrogel in the Rh B adsorption reactions. The adsorption reaction was carried out with p(AMPS-Na$^+$-*co*-VIm) hydrogel under the same reaction conditions. Since the pores of the p(AMPS-H$^+$-*co*-VIm) hydrogel were smaller than those of the p(AMPS-Na$^+$-*co*-VIm) hydrogel, the adsorption efficiency of Rh B was lower for the p(AMPS-H$^+$-*co*-VIm) hydrogel. Therefore, the great adsorption efficiency of p(AMPS-Na$^+$-*co*-VIm) hydrogels can be attributed to their favorable porous structure. The distribution of Rh B molecules and solvents in p(AMPS-Na+-*co*-VIm) pores is greater than that in p(AMPS-H$^+$-*co*-VIm) pores. Consequently, active adsorption sites are less accessible in p(AMPS-H$^+$-*co*-VIm) hydrogels than in p(AMPS-Na$^+$-*co*-VIm) hydrogels.

In the same way, p(AMPS-H$^+$-*co*-VIm)-Ag compounds tend to have greater catalytic activity than bare hydrogels p(AMPS-H$^+$-*co*-VIm). The adsorption capacity was 38.6 mg/g and 45.4 mg/g, for p(AMPS-H$^+$-*co*-VIm) and p(AMPS-H$^+$-*co*-VIm)-Ag, respectively.

In the current study, the role of quaternizing p(AMPS-Na$^+$-*co*-VIm) hydrogels in the adsorption behavior of Rh B was also examined. The same amount of the quternized hydrogel was inserted in the aqueous solution of Rh B (40 ppm) at room temperature. The results revealed that the quternized hydrogel yielded a greater adsorption capacity for Rh B (60.2 mg/g) than the non-quternized hydrogel. It can be stated that the hydrophobicity and flexibility of the quaternized hydrogel enhanced in the aqueous solution, which improved π-π interactions among the aromatic compounds of VIm and Rh B and eventually increased the uptake of Rh B in this hydrogel. To be more precise, with an increment in the flexibility of alkyl chains, the imidazole groups easily rotated, which enhanced the possibility of π-type interactions between the Rh B molecules and the imidazole ring. The quaternized hydrogel adsorbed a greater amount of Rh B molecules due to the formation of electrostatic bonds between Br- and cationic dye. Other contributing factors to the adsorption behavior of Rh B on the surface of the quaternized hydrogel are as follows: the electron donor-electron acceptor interaction between $OH^{-\delta}$ and N^+ in the qauternized hydrogel, anion-π

interactions between Br^- and the aromatic ring of Rh B, H-bonding between CH_3 and O atoms, electrostatic bonding, and CH-π interactions between alkyl chains and the aromatic ring of Rh B [33].

CONCLUSION

Diverse hydrogels synthesized by changing the pH of reaction media, turning into neutral or basic. Regarding the reaction condition, different behaviors in terms of porosity, metal amount loading, dye removal were observed for p(AMPS-Na^+-*co*-VIm) and p(AMPS-H^+-*co*-VIm) hydrogels. Notably, the higher removal efficiency of cationic dyes makes our ionogels complementary to other imidazolium-based gels in which these ion gels can display higher removal performance in the presence of anionic dyes. The attempt to correlate the performance of hydrogel phases to their structural features highlights that the morphology of materials plays a significant role in determining the adsorption ability. More importantly, these catalysts have high stability and easy recyclability. This study offers a new method for preparing precious metal nanoparticle catalysts which have great potential as highly effective and stable catalysts in water treatment.

CONFLICT OF INTEREST

The authors declare that there are no conflicts of interest regarding the publication of this paper.

ACKNOWLEDGMENTS

The authors are grateful to the University of Zanjan for financial support of this study.

REFERENCES

[1] Marullo S, Rizzo C, Dintcheva NT, Giannici F, D'Anna F. Ionic liquids gels: Soft materials for environmental remediation. Journal of Colloid and Interface Science. 2018;517:182-93. https://doi.org/10.1016/j.jcis.2018.01.111

[2] Sepehri A, Sarrafzadeh M-H. Effect of nitrifiers community on fouling mitigation and nitrification efficiency in a membrane bioreactor. Chemical Engineering and Processing - Process Intensification. 2018;128:10-8. https://doi.org/10.1016/j.cep.2018.04.006

[3] Carolin CF, Kumar PS, Saravanan A, Joshiba GJ, Naushad M. Efficient techniques for the removal of toxic heavy metals from aquatic environment: A review. Journal of Environmental Chemical Engineering. 2017;5(3):2782-99. https://doi.org/10.1016/j.jece.2017.05.029

[4] Sinha V, Chakma S. Advances in the preparation of hydrogel for wastewater treatment: A concise review. Journal of Environmental Chemical Engineering. 2019;7(5):103295. https://doi.org/10.1016/j.jece.2019.103295

[5] Atta MA, Al-Lohdan HA, Ezzat AO, Tawfik AM, Hashem AI. Synthesis of zinc oxide nanocomposites using poly (ionic liquids) based on quaternary ammonium acrylamidomethyl propane sulfonate for water treatment. Journal of Molecular Liquids. 2017; 236:38-47. https://doi.org/10.1016/j.molliq.2017.04.012

[6] Hamedi H, Moradi S, Hudson SM, Tonelli AE. Chitosan based hydrogels and their applications for drug delivery in wound dressings: A review. Carbohydrate Polymers. 2018;199:445-60. https://doi.org/10.1016/j.carbpol.2018.06.114

[7] Caló E, Khutoryanskiy VV. Biomedical applications of hydrogels: A review of patents and commercial products. European Polymer Journal. 2015;65:252-67. https://doi.org/10.1016/j.eurpolymj.2014.11.024

[8] Guilherme MR, Aouada FA, Fajardo AR, Martins AF, Paulino AT, Davi MFT, et al. Superabsorbent hydrogels based on polysaccharides for application in agriculture as soil conditioner and nutrient carrier: A review. European Polymer Journal. 2015;72:365-85. https://doi.org/10.1016/j.eurpolymj.2015.04.017

[9] Thakur S, Govender PP, Mamo MA, Tamulevicius S, Mishra YK, Thakur VK. Progress in lignin hydrogels and nanocomposites for water purification: Future perspectives. Vacuum. 2017;146:342-55. https://doi.org/10.1016/j.vacuum.2017.08.011

[10] Tang C-Y, Yu P, Tang L-S, Wang Q-Y, Bao R-Y, Liu Z-Y, et al. Tannic acid functionalized graphene hydrogel for organic dye adsorption. Ecotoxicology and Environmental Safety. 2018;165:299-306. https://doi.org/10.1016/j.ecoenv.2018.09.009

[11] Haleem A, Syaal SB, Ajmal M, Ambreen J, Rauf S, Ali N, et al. Silver and palladium nanoparticle embedded poly(n-isopropylacrylamide-co-2-acrylamido-2-methylpropane sulfonic acid) hybrid microgel catalyst with pH and temperature dependent catalytic activity. Korean Journal of Chemical Engineering. 2020;37(4):614-22. https://doi.org/10.1007/s11814-020-0484-7

[12] Mittal H, Kumar V, Saruchi, Ray SS. Adsorption of methyl violet from aqueous solution using gum xanthan/Fe3O4 based nanocomposite hydrogel. International Journal of Biological Macromolecules. 2016;89:1-11. https://doi.org/10.1016/j.ijbiomac.2016.04.050

[13] Marandi GB, Kermani ZP, Kurdtabar M. Fast and Efficient Removal of Cationic Dyes From Aqueous Solution by Collagen-Based Hydrogel Nanocomposites. Polymer-Plastics Technology and Engineering. 2013;52(3):310-8. https://doi.org/10.1080/03602559.2012.748806

[14] Kurdtabar M, Peyvand Kermani Z, Bagheri Marandi G. Synthesis and characterization of collagen-based hydrogel nanocomposites for adsorption of Cd2+, Pb2+, methylene green and crystal violet. Iranian Polymer Journal. 2015;24(9):791-803. https://doi.org/10.1007/s13726-015-0368-6

[15] Ortega A, Bucio E, Burillo G. New Interpenetrating Polymer Networks of N-isopropylacrylamide/N-acryloxysuccinimide: Synthesis and Characterization. Polymer Bulletin. 2008;60(4):515-24. https://doi.org/10.1007/s00289-007-0870-x

[16] Lin S-B, Yuan C-H, Ke A-R, Quan Z-L. Electrical response characterization of PVA-P(AA/AMPS) IPN hydrogels in aqueous Na2SO4 solution. Sensors and Actuators B: Chemical. 2008;134(1):281-6.

https://doi.org/10.1016/j.snb.2008.04.045
[17] Durmaz S, Okay O. Acrylamide/2-acrylamido-2-methylpropane sulfonic acid sodium salt-based hydrogels: synthesis and characterization. Polymer. 2000;41(10):3693-704. https://doi.org/10.1016/S0032-3861(99)00558-3
[18] Liu K, Qin T, Sun Y, Hou C, Cao X, Jiang S. Synergistic effect between Ag and Mn3O4 in the gas phase oxidation of alcohols. Catalysis Communications. 2018;113:15-8. https://doi.org/10.1016/j.catcom.2018.05.002
[19] Jia L, Zhang S, Gu F, Ping Y, Guo X, Zhong Z, et al. Highly selective gas-phase oxidation of benzyl alcohol to benzaldehyde over silver-containing hexagonal mesoporous silica. Microporous and Mesoporous Materials. 2012;149(1):158-65. https://doi.org/10.1016/j.micromeso.2011.08.009
[20] Genç F, Uzun C, Güven O. Quaternized poly(1-vinylimidazole) hydrogel for anion adsorption. Polymer Bulletin. 2016;73(1):179-90. https://doi.org/10.1007/s00289-015-1479-0
[21] Kousha M, Daneshvar E, Sohrabi MS, Jokar M, Bhatnagar A. Adsorption of acid orange II dye by raw and chemically modified brown macroalga Stoechospermum marginatum. Chemical Engineering Journal. 2012;192:67-76. https://doi.org/10.1016/j.cej.2012.03.057
[22] Adebayo MA, Prola LDT, Lima EC, Puchana-Rosero MJ, Cataluña R, Saucier C, et al. Adsorption of Procion Blue MX-R dye from aqueous solutions by lignin chemically modified with aluminium and manganese. Journal of Hazardous Materials. 2014;268:43-50. https://doi.org/10.1016/j.jhazmat.2014.01.005
[23] Tang L, Cai Y, Yang G, Liu Y, Zeng G, Zhou Y, et al. Cobalt nanoparticles-embedded magnetic ordered mesoporous carbon for highly effective adsorption of rhodamine B. Applied Surface Science. 2014;314:746-53. https://doi.org/10.1016/j.apsusc.2014.07.060
[24] Xu X, Chen S, Wu Q. Surface molecular imprinting on polypropylene fibers for rhodamine B selective adsorption. Journal of Colloid and Interface Science. 2012;385(1):193-201. https://doi.org/10.1016/j.jcis.2012.07.013
[25] Anandkumar J, Mandal B. Adsorption of chromium(VI) and Rhodamine B by surface modified tannery waste: Kinetic, mechanistic and thermodynamic studies. Journal of Hazardous Materials. 2011;186(2):1088-96. https://doi.org/10.1016/j.jhazmat.2010.11.104
[26] Zhou Y, Zhang M, Hu X, Wang X, Niu J, Ma T. Adsorption of Cationic Dyes on a Cellulose-Based Multicarboxyl Adsorbent. Journal of Chemical & Engineering Data. 2013;58(2):413-21. https://doi.org/10.1021/je301140c
[27] Tang Y, He T, Liu Y, Zhou B, Yang R, Zhu L. Sorption behavior of methylene blue and rhodamine B mixed dyes onto chitosan graft poly (acrylic acid-co-2-acrylamide-2-methyl propane sulfonic acid) hydrogel. Advances in Polymer Technology. 2018;37(7):2568-78. https://doi.org/10.1002/adv.21932
[28] Shukla NB, Madras G. Adsorption of cationic dyes on poly(acrylic acid-co-sodium acrylate-co-acrylamide) superabsorbents. Journal of Applied Polymer Science. 2012;124(5):3892-9. https://doi.org/10.1002/app.35479
[29] Liu Y, Zheng Y, Wang A. Enhanced adsorption of Methylene Blue from aqueous solution by chitosan-g-poly (acrylic acid)/vermiculite hydrogel composites. Journal of Environmental Sciences. 2010;22(4):486-93. https://doi.org/10.1016/S1001-0742(09)60134-0
[30] Lim Teik Zheng A, Phromsatit T, Boonyuen S, Andou Y. Synthesis of silver nanoparticles/porphyrin/reduced graphene oxide hydrogel as dye adsorbent for wastewater treatment. FlatChem. 2020;23:100174. https://doi.org/10.1016/j.flatc.2020.100174
[31] Aboelfetoh EF, Gemeay AH, El-Sharkawy RG. Effective disposal of methylene blue using green immobilized silver nanoparticles on graphene oxide and reduced graphene oxide sheets through one-pot synthesis. Environmental Monitoring and Assessment. 2020;192(6):355. https://doi.org/10.1007/s10661-020-08278-2
[32] Salem MA, Elsharkawy RG, Hablas MF. Adsorption of brilliant green dye by polyaniline/silver nanocomposite: Kinetic, equilibrium, and thermodynamic studies. European Polymer Journal. 2016;75:577-90. https://doi.org/10.1016/j.eurpolymj.2015.12.027
[33] Abou-Zeid RE, Awwad NS, Nabil S, Salama A, Youssef MA. Oxidized alginate/gelatin decorated silver nanoparticles as new nanocomposite for dye adsorption. International Journal of Biological Macromolecules. 2019;141:1280-6. https://doi.org/10.1016/j.ijbiomac.2019.09.076
[34] Yao G, Bi W, Liu H. pH-responsive magnetic graphene oxide/poly(NVI-co-AA) hydrogel as an easily recyclable adsorbent for cationic and anionic dyes. Colloids and Surfaces A: Physicochemical and Engineering Aspects. 2020;588:124393. https://doi.org/10.1016/j.colsurfa.2019.124393
[35] Toledo PVO, Bernardinelli OD, Sabadini E, Petri DFS. The states of water in tryptophan grafted hydroxypropyl methylcellulose hydrogels and their effect on the adsorption of methylene blue and rhodamine B. Carbohydrate Polymers. 2020;248:116765. https://doi.org/10.1016/j.carbpol.2020.116765
[36] Karimi-Maleh H, Ranjbari S, Tanhaei B, Ayati A, Orooji Y, Alizadeh M, et al. Novel 1-butyl-3-methylimidazolium bromide impregnated chitosan hydrogel beads nanostructure as an efficient nanobio-adsorbent for cationic dye removal: Kinetic study. Environmental Research. 2021;195:110809. https://doi.org/10.1016/j.envres.2021.110809